JOURNAL OF AIRCRAFT
Vol. 41, No. 2, March–April 2004

Aerodynamic Shape Design of Rotor Airfoils Undergoing Unsteady Motion

Yushin Kim* and Kwanjung Yee†
Korea Aerospace Research Institute, Daejun 305-333, Republic of Korea
and
Dong-Ho Lee‡
Seoul National University, Seoul 151-742, Republic of Korea

A new design method is suggested that can handle the dynamic response of an airfoil subjected to unsteady motion and flow conditions. A new objective function and constraints are defined to represent the overall characteristics of the rotor airfoil over a single cycle. A weighting function is also introduced to enable a designer to determine the specific azimuthal location at which the performance is improved intensively. A numerical analysis code that can handle the oscillatory pitching motion of an airfoil and the inflow Mach number variation is developed. The analyses during the design process are limited to the cases without dynamic stall because the numerical analysis code cannot predict the dynamic stall phenomena with sufficient accuracy. Response surface methodology is exclusively employed to construct and optimize the response surface models of the objective functions and constraints. The advantages of the method are demonstrated by a comprehensive comparison with a static three-point design method. The dynamic method can yield a better airfoil for the following reasons: 1) The static performance is not always proportional to the dynamic performance. 2) The moment constraint used in the static three-point design is too tight to allow enough variation of the design variables. 3) The objective function of the static three-point design may be implicitly overweighted at a certain design point so that the overall aerodynamic performance is miscalculated, unlike in the present method. The variations of the aerodynamic performance with weighting functions are also discussed.

Nomenclature

C	=	coefficient matrix in response surface model
C_l, C_m	=	aerodynamic lift and pitching moment coefficients, respectively
c	=	chord length
$\hat{\boldsymbol{F}}, \hat{\boldsymbol{G}}$	=	inviscid flux vector
$\hat{\boldsymbol{F}}_v, \hat{\boldsymbol{G}}_v$	=	viscous flux vector
F_c	=	constraint
F_o	=	objective function
J	=	Jacobian
k	=	reduced frequency, $\omega c/2U_\infty$
L/D	=	lift-to-drag ratio
M_m	=	amplitude of freestream Mach number variation
M_0	=	mean Mach number
M_∞	=	freestream Mach number
n_s	=	number of numerical experiments
n_t	=	number of coefficients in response surface model
n_v	=	number of design variables
$\hat{\boldsymbol{Q}}$	=	vector of conservative variables
Re_c	=	Reynolds number based on chord length
α	=	angle of attack, deg
α_m	=	amplitude of pitching motion, deg
α_{ref}	=	reference angle of attack at which weighting is maximum
α_0	=	mean angle, deg
ε	=	error in response surface model
$\hat{\sigma}^2$	=	estimation of variance
ψ	=	azimuth angle

Superscript

T	=	transpose of matrix

Received 12 April 1999; presented as Paper 99-3107 at the AIAA 17th Applied Aerodynamic conference, Norfolk, VA, 28 June 1999–1 July 1999; revision received 1 April 2003; accepted for publication 27 April 2003.

*Senior Researcher.
†Senior Researcher.
‡Professor, School of Mechanical and Aerospace Engineering. Senior Member AIAA.

Introduction

IN the early 1970s, it was recognized that choosing a better airfoil that delays dynamic stall while satisfying other constraints could significantly enhance overall rotor performance.[1] Since then, a database on the unsteady rotor flow field, especially on dynamic stall has been accumulated through various experimental and theoretical research.[2,3] However, the database itself is not able to provide systematic guidelines for selecting proper airfoils, and the design process of these airfoils still depends on the physical insight and experience of a designer. Although many design studies are available for steady transonic airfoils, limited research has been carried out on rotor airfoil design.[4–10] There are several reasons that rotor airfoil design has remained one of the most challenging problems for past years.

First, the flowfield around a rotor section is essentially unsteady and very complex for numerical analysis. A rotor section in forward flight undergoes periodic unsteady flow condition and motion as shown in Fig. 1. At the advancing side, compressibility effects associated with shock waves result in a sudden increase of wave drag, which leads to high profile power, blade loads, vibration, and noises. At the retreating side, characterized by high angle of attack and low relative velocity, dynamic stall accompanied by massive separation causes aerodynamic instability and control problems. Accordingly, the airfoil characteristics required for each flow regime are quite different and often contradictory. To yield an appropriate design output, the numerical analysis code should have sufficient accuracy. However, the numerical solution for the flowfield that has high angle of attack and some separation has been significantly different from the experimental data up to now.[2,11] This difference is partly due to having no reliable turbulence models

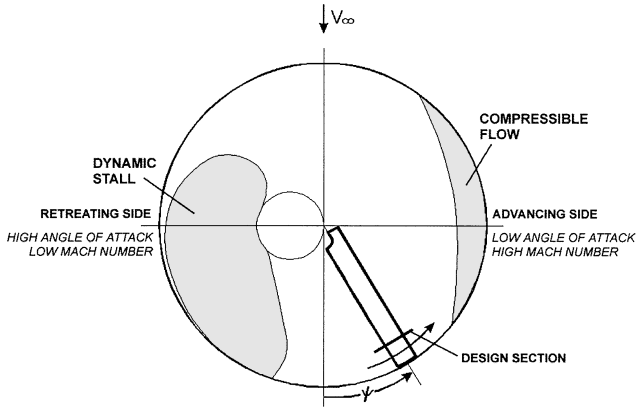

Fig. 1 Aerodynamic environment of a helicopter rotor blade in forward flight.

for massive separation. Fortunately, most of the present-day helicopters are operated under light and onset stall conditions, in which separation is not as severe as it is in deep stall conditions, and the geometric shape of the airfoil has great influence on the overall flowfield.[2] The design flow condition in this study, therefore, does not involve dynamic stall, and the reason for this is that the numerical analysis code developed and used in this study cannot predict the light and deep dynamic stall phenomena with sufficient accuracy.

Second, a typical numerical analysis is extremely time consuming. One reason for this is that a numerical analysis code should have high fidelity to capture complex flow physics such as shock waves and separation. Another reason is that the computation continues until a periodic solution is obtained. To overcome these difficulties, a minimum number of design variables should be used, and a new computational strategy such as parallel computing is required.[12]

Third, most airfoil design procedures are devised to optimize the steady performance of an airfoil, and therefore, they cannot consider unsteady dynamic effects.[4–6] Because the dynamic characteristics of an airfoil do not necessarily coincide with the static ones, a design procedure should be able to handle the dynamic response of an airfoil in unsteady motion. In recent years, there have been several attempts to obtain a rotor airfoil that has optimal performance under realistic flow conditions.[7–10] However, most previous design studies are essentially multipoint designs that optimize static characteristics at several different flow conditions and are not able to include dynamic characteristics of the airfoil responding to the continuously varying flow condition.

The objectives of the present paper are as follows: 1) suggest a new design procedure that can handle the dynamic response of an airfoil undergoing unsteady motion and flow conditions; 2) demonstrate the advantages of the present design method as well as the limitation of the multipoint design by comparison with static three-point design; and 3) discuss the variations of the aerodynamic performance according to the weighting values.

To achieve these goals, two-dimensional full Navier–Stokes equations that can handle dynamic grid motion are employed for unsteady flow field analyses. Both the Mach number and incidence angle are allowed to vary simultaneously to represent a real flow environment.[13,14] A simple algebraic turbulence model is used because the problem under consideration is below the static stall angle.[15] For numerical optimization, response surface methodology (RSM) is employed to construct the numerical models for the objective function and constraints. A new objective function is defined to represent the overall aerodynamic performance such as L/D over a single cycle, and a weighting function is introduced to enable a designer to specify an azimuthal location at which the performance of the airfoil is maximized. RSM is a kind of modeling method based on design of experiment theory. In this method, a designer performs a limited number of computational analyses using experimental design theory to prescribe values for independent variables. With the resulting data, the designer creates mathematical models using some type of function. The designer then uses the response surface (RS) model in subsequent calculations during the optimization process.[12,16–18]

Numerical Methods

The conservative form of the compressible, Reynolds-averaged, Navier–Stokes equations for a body-fitted coordinate system is used as follows[19]:

$$\partial_t \hat{\boldsymbol{Q}} + \partial_\xi \hat{\boldsymbol{F}} + \partial_\eta \hat{\boldsymbol{G}} = Re_c^{-1}(\partial_\xi \hat{\boldsymbol{F}}_v + \partial_\eta \hat{G}_v) \tag{1}$$

where $\hat{\boldsymbol{Q}} = J^{-1}[\rho, \rho u, \rho v, \rho e]^T$ is the conservative variable vector, $\hat{\boldsymbol{F}}$ and $\hat{\boldsymbol{G}}$ are flux vectors, and $\hat{\boldsymbol{F}}_v$ and $\hat{G}_v$ are viscous terms. All geometrical dimensions are normalized with the airfoil chord length c, the density is normalized with the freestream value ρ_∞, the Cartesian velocity components are normalized with the freestream speed of sound, and the pressure p is normalized with the freestream value. The upwind-biased, factorized, iterative, implicit numerical scheme is used to compute the mean flow. The inviscid flux vectors $\hat{\boldsymbol{F}}$ and $\hat{\boldsymbol{G}}$ are evaluated using Roe's upwind scheme. For higher-order spatial accuracy, the MUSCL approach is adopted with a Koren limiter. The Newtonian subiteration method defined in Eq. (2) is introduced to restore the temporal accuracy to second order as well as to minimize the factorization error:

$$\frac{\partial \hat{Q}^{n+1,s+1}}{\partial \tau} = C_0 \hat{Q}^{n+1,s+1} + C_1 \hat{Q}^n + C_2 \hat{Q}^{n-1}$$

$$C_0 = \frac{1-\sigma}{(1-\sigma)\Delta t_2 + \Delta t_1}, \qquad C_1 = \frac{\sigma}{(1-\sigma)\Delta t_2 + \Delta t_1}$$

$$C_2 = \frac{-1}{(1-\sigma)\Delta t_2 + \Delta t_1}, \qquad \sigma = \left(1 + \frac{\Delta t_2}{\Delta t_1}\right)^2$$

$$\Delta t_1 = t^n - t^{n-1}, \qquad \Delta t_2 = t^{n+1} - t^n \tag{2}$$

The boundary conditions are specified as follows. On the solid wall, the velocity is specified to the airfoil velocity to consider the time-dependent unsteady grid motions. The pressure on the wall is evaluated from the normal momentum equation. At the inflow, freestream conditions are specified for velocity and pressure, and one-dimensional Riemann invariant extrapolation is used to obtain the density. At the outflow, freestream pressure is specified, and one-dimensional Riemann invariants are used to obtain the velocities and the density from the interior. For turbulence, the widely used algebraic Baldwin–Lomax turbulence model[15] is used with a modification to account for the unsteady motion. The Baldwin–Lomax turbulence model is not applicable to the region of massive separation, but in the flow conditions under consideration, it is known to yield sufficiently accurate solutions.[15]

RSM

In many RSM analyses, quadratic polynomials are used to model the observed responses accurately, although it is certainly not true for all cases. If n_s analyses are carried out, then the quadratic RS model can be written as

$$y^{(p)} = c_0 + \sum_{1 \le i \le n_v} c_i x_i^{(p)} + \sum_{1 \le i \le j \le n_v} c_{ij} x_i^{(p)} x_j^{(p)} + \varepsilon$$

$$p = 1, \ldots, n_s \tag{3}$$

where $y^{(p)}$ is the response; $x_i^{(p)}$ and $x_j^{(p)}$ are the n_v design variables; c_0, c_i, and c_{ij} are unknown coefficients; and ε is an error.

Note that the quadratic polynomials have $n_t = (n_v + 1)(n_v + 2)/2$ coefficients and that this model can be written in matrix notation as

$$y^{(p)} = \bar{x}^{(p)} C, \qquad C = [c_0, c_1, \ldots, c_{n_t - 1}]^T \tag{4}$$

Estimating the unknown coefficients requires n_s analyses, where $n_s \ge n_t$. Under such conditions, the estimation problem is formulated in matrix notation as

$$\boldsymbol{y} \approx \boldsymbol{X} C, \qquad \boldsymbol{y} = [y^{(1)}, y^{(2)}, \ldots, y^{(n_s)}]^T$$

$$\boldsymbol{X} = \begin{bmatrix} 1 & x_1^{(1)} & x_2^{(1)} & \cdots & \left(x_{n_v}^{(1)}\right)^2 \\ \vdots & \vdots & \vdots & \ddots & \vdots \\ 1 & x_1^{(n_s)} & x_2^{(n_s)} & \cdots & \left(x_{n_v}^{(n_s)}\right)^2 \end{bmatrix} \tag{5}$$

The unique least-square solution to Eq. (5) is given as

$$\hat{C} = (\boldsymbol{X}^T\boldsymbol{X})^{-1}\boldsymbol{X}^T\boldsymbol{y} \tag{6}$$

When $\hat{C}$ is substituted for C into Eq. (4), the values of the response may be predicted at any location $\bar{x}$ by mapping $\bar{x}$ into $\bar{x}^{(p)}$. In matrix notation, this can be written as

$$\hat{y} = \bar{x}\hat{C} \tag{7}$$

More details are given in Ref. 18.

A proper selection of numerical experimental points in design space plays an important role in the overall accuracy of the resulting RS model. There are several methods to select these candidate points, for example, the full-factorial design method and the central-composite design method. However, because those methods are intended for use with a rectangular design space and not irregularly shaped design space and because they become impractical as n_v becomes greater than 10, the D-optimal experimental design is used in the present research. It requires fewer response values than a central-composite experimental design and has proven to be particularly suitable for the irregularly shaped design space that may arise in the present design problem.[12,16–18] The DOPT code developed at Carnegie–Melon University is employed for the D-optimal experimental design in the present paper.

After the coefficients in the RS model are estimated, analysis of variance and regression analysis produce a measure of uncertainty in the coefficients. This uncertainty estimation is provided by t-static defined as

$$t = c_{j-1}\Big/\sqrt{\hat{\sigma}^2(X^TX)^{-1}_{jj}}, \qquad j = 1, \ldots, n_t \tag{8}$$

where $\hat{\sigma}^2$ is the estimation of variance. Low values of t-static represent an inaccurate coefficient. Allowing poorly estimated terms to remain in the RS model may reduce the prediction accuracy of the model. A common measure of the utility of removing terms from the RS model is the adjusted R^2 that is calculated using the error sum of squares (SSE), total sum of squares (SYY), and degrees of freedom (DOF) as

$$R^2_{\text{adj}} = 1 - \frac{\text{SSE}/\text{DOF}_{\text{SSE}}}{\text{SYY}/\text{DOF}_{\text{SYY}}} \tag{9}$$

Typical values of R^2_{adj} range from 0.9 to 1.0 when the observed response values are accurately predicted. Of the several methods to remove the unnecessary terms from the full RS model, all possible regression and stepwise regression are generally used. In the present work, mixed regression is employed, which is a kind of stepwise regression. A new RS model obtained from regression analysis is called a reduced model. More details are given in Ref. 18.

The optimization process using RSM is summarized in the flowchart of Fig. 2.

Geometric Representation of Airfoil

A common way to represent the geometry of an airfoil is to employ shape functions or spline curves. However, these functions or curves usually require more than 20 design variables to yield accurate geometric representation, and this is a serious computational burden. When analytic functions are used such as those that define NACA series airfoils, less than five design variables are sufficient to represent the geometry. It is practical and advantageous to keep the number of design variables to a minimum in any design method because this drastically reduces the amount of analysis or experiment. In this work, a NACA modified four-digit series airfoil is chosen, to keep the number of design variables as small as possible, thereby reducing overall computational time.

The NACA modified four-digit series airfoil is defined as NACA *MPXX-IT*. M specifies the maximum camber in percentage of the chord, P indicates the position of the maximum camber in tenths of chord, and XX provides the maximum thickness of the airfoil in percentage of chord. I, the first digit following the dash, refers to the roundedness of the nose. A value of 6 indicates that the nose radius is the same as the original airfoil, whereas a value of 0 indicates a sharp leading edge. Increasing this value specifies an increasingly more rounded nose. T determines the location of maximum thickness in tenths of chord.

Table 1 Ranges of design variables

Range	M	P	XX	I	T
Minimum	0.05	1.5	10	5.7	2.5
Maximum	2	2.5	13	6.22	3.5
AMES-01	1.33	1.830	10.62	6.0120	3.282

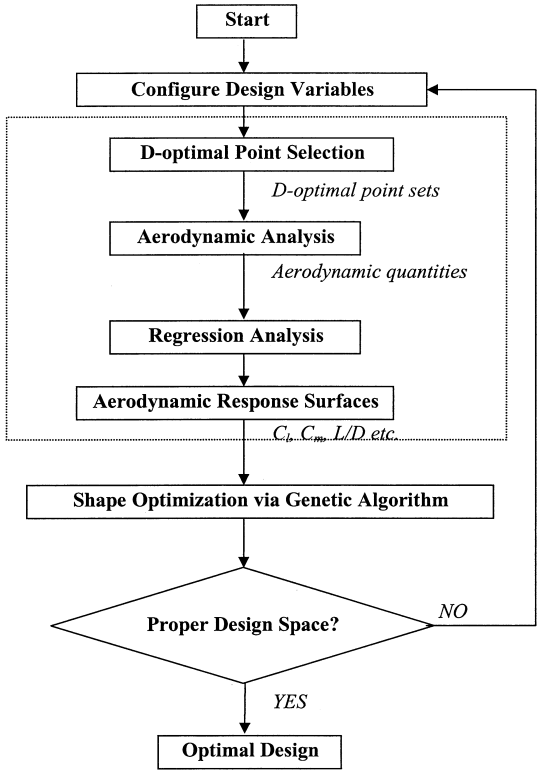

Fig. 2 Design procedure of a rotor airfoil using response surface methodology.

The total number of design variables is 5, and about 50 calculations are sufficient to produce accurate RS models.[18] The ranges of design variables, determined by approximating the AMES-01 airfoil with the NACA modified four-digit series airfoil, are shown in Table 1 and Fig. 3. The baseline airfoil takes the middle values between the upper and lower limits.

Combined Motion of Airfoil

Unsteady effects generated on the retreating side of a helicopter blade have been extensively investigated in past years to improve the predictability of local aerodynamic behavior as well as overall performance. Although a proper simulation of the complex rotor flowfield requires simultaneous fluctuations of velocity and incidence of the incoming freestream, most past studies have tackled the problem by separating the influence of these combined effects, with the exception of the work of Favier et al.[13,14] Arbitrary incidence and velocity fluctuations can be written as Fourier series as follows[13]:

$$V(t) = V_\infty + \sum_{k=1}^{n} V_k \sin\left(k\omega t + \Phi_k^v\right) \tag{10}$$

$$\alpha(t) = \alpha_0 + \sum_{k=1}^{n} \alpha_k \sin\left(k\omega t + \Phi_k^\alpha\right) \tag{11}$$

where Φ_k^v and Φ_k^α are phase shifts.

Table 2 Flow conditions for static three-point design

Parameter	$\psi = 90$ deg ($i = 1$)	$\psi = 180$ deg ($i = 2$)	$\psi = 270$ deg ($i = 3$)
Re_c	4.585×10^6	3.017×10^6	1.448×10^6
Mach number	0.731	0.481	0.231
α, deg	1.5	5.5	9.5

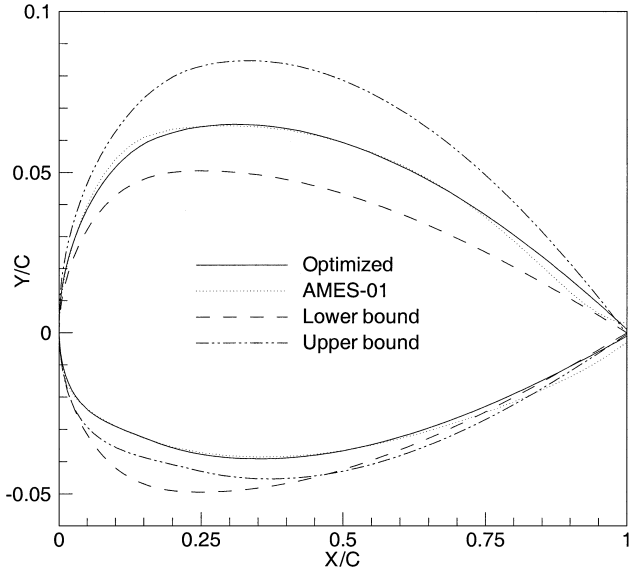

Fig. 3 Ranges of the design variables for numerical optimization.

In general, three to four airfoils are implemented at the helicopter blade along the span, and the design requirements are different for each airfoil. The design flow conditions are specified based on the Messerschmitt-Bolkow-Blohm (MBB) BO 105 rotor blade section at the 75% spanwise location that is in forward flight with about 300 km/h as indicated. Then, Mach number and angle of attack (in degrees) are considered to vary as follows:

$$M_\infty = M_0 - M_m \sin(\omega t), \qquad M_0 = 0.481, \qquad M_m = 0.25$$
$$\alpha = \alpha_0 + \alpha_m \sin(\omega t), \qquad \alpha_0 = 5.5, \qquad \alpha_m = 4$$
$$k = \omega c/2U_\infty = 0.037, \qquad Re_c = 3.017 \times 10^6 \qquad (12)$$

Hence, the velocity has a minimum value of $M_\infty = 0.231$ at the maximum incidence of 9.5 deg, and at the minimum incidence of 1.5 deg, the velocity reaches a maximum of $M_\infty = 0.731$. Note that all aerodynamic coefficients are normalized with the instantaneous dynamic pressure. Figure 4 shows the surface pressure distributions for six different phase angles during the downstroke for the given unsteady design conditions. The developed unsteady numerical analysis code is used to solve the unsteady flowfield around the baseline airfoil. As clearly shown in Fig. 4, the pressure distribution plots vary smoothly during the downstroke and do not exhibit dynamic stall behavior because the reduced frequency, amplitude of the angle of attack variation, and the maximum incidence are not sufficiently high enough to incur dynamic stall.

In view of the hovering flight conditions, the angle of attack of the rotor blade during the hovering flight is approximately 6–9 deg at the 75% spanwise location, and the specified flow conditions cover that angle of attack. The hovering flight conditions, therefore, are included implicitly and partly in the specified unsteady flow conditions.

The design flow conditions for the static three-point design at azimuth angle $\psi = 90$, 180, and 270 deg are shown in Table 2. The flow conditions are also specified based on the MBB BO 105 rotor blade section at the 75% spanwise location.

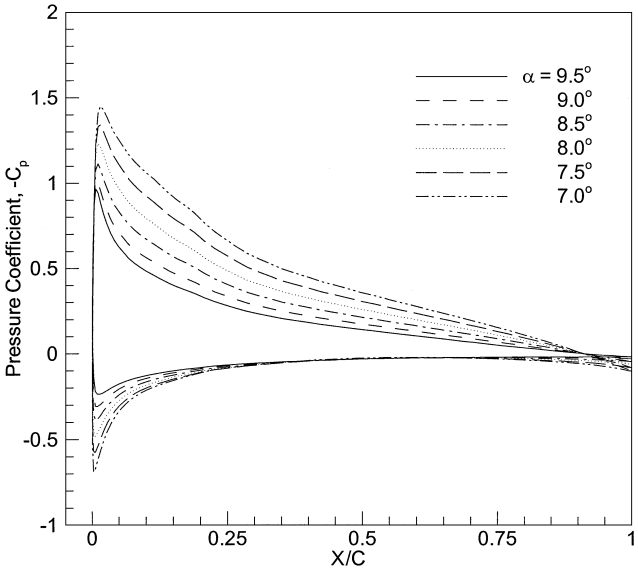

Fig. 4 Surface pressure distributions during the downstroke for the unsteady design flow conditions: M_∞ = 0.481–0.25 sin(ωt), α = 5.5 + 4 sin(ωt), $k = \omega c/2U_\infty$ = 0.037, and $Re_c = 3.017 \times 10^6$.

Results and Discussion

Validation of Aerodynamic Analysis

To validate the accuracy of the developed unsteady numerical analysis code, the unsteady transonic flowfield around a NACA 0012 airfoil in periodic pitching motion was evaluated and compared with the experimental data of Landon.[20] The comparison was made for constant transonic inflow because the experimental data were not available to deal with the simultaneous variation of inflow velocity and incidence. Favier's experiments were conducted at low Reynolds number and cannot be used for comparison.[13,14] The flow conditions are given as

$$\alpha = \alpha_0 + \alpha_m \sin(\omega t), \qquad \alpha_0 = 4.86, \qquad \alpha_m = 2.44$$
$$M_\infty = 0.6, \qquad Re_c = 4.8 \times 10^6, \qquad k = \omega c/2U_\infty = 0.08 \qquad (13)$$

The flow for this motion is initially subsonic, but as the angle of attack increases to about 5 deg, a supersonic flow region develops around the leading edge and a transonic shock appears. This shock remains during the upstroke until the maximum angle of attack is reached and during the downstroke to about $\alpha \approx 5$ deg. This flow condition was selected to verify the capability of the present numerical analysis code to handle the transonic problem.

A typical grid used for the numerical analyses is shown in Fig. 5. A C-type grid (239×61) was used for all numerical analyses, and 141 points were distributed on the airfoil surface. The spacing between the airfoil surface and the center of the first cell in the direction normal to the airfoil surface was set to 2×10^{-5} chords, which ensured an average Y^+ of roughly one for the Reynolds number of about 4×10^6.

The computed and measured lift and pitching moment history are compared in Figs. 6a and 6b, respectively. The computed lift and pitching moment coefficients closely agreed with the measured values. Figure 7 shows a comparison of the computed surface pressure distribution and the experimental data from Landon[20] for two angles during the upstroke and two angles during the downstroke. The computed pressure distribution agreed well with the measurements in all cases. There was a little discrepancy between the calculated and measured shock positions during the downstroke, but the overall characteristics were well predicted with sufficient accuracy.

Table 3 Ranges of design variables for inverse design

Range	M	P	XX	I	T
Minimum	0.6	1.8	11	5.87	2.8
Maximum	1.4	2.2	12	6.05	3.2

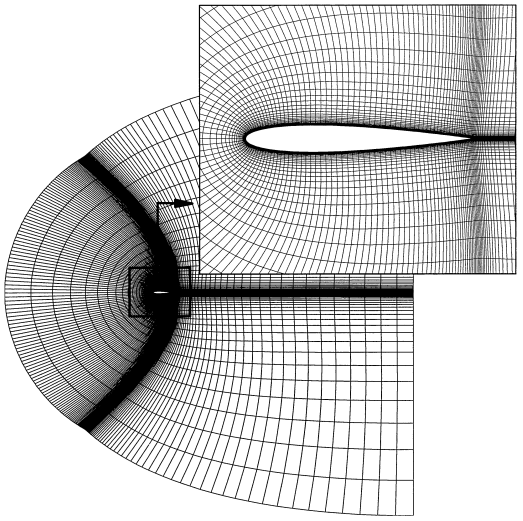

Fig. 5 Typical grid over a NACA 0012 airfoil used for numerical analyses (239 × 61).

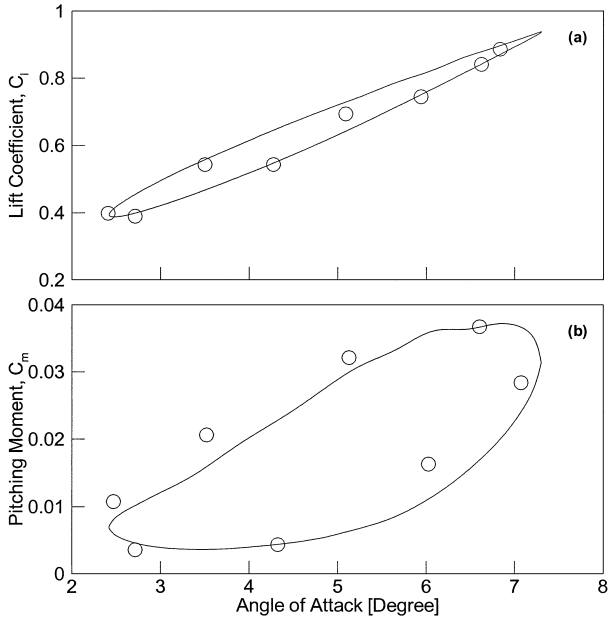

Fig. 6 Comparison of the measured and computed coefficients for oscillatory pitching motion for $M_\infty = 0.6$, $\alpha = 4.86 + 2.44\sin(\omega t)$, $k = \omega c/2U_\infty = 0.08$, and $Re_c = 4.8 \times 10^6$: a) lift and b) pitching moment: ○, measured and ——, computed.

Validation of Design Method via Inverse Design

As described in the preceding section, the numerical optimization via RSM employs approximate numerical models, called the RS models, obtained from a limited number of numerical experiments. Now, the question is whether the numerical optimization, using the RS models, can really find the global optimum within the design space. If the design procedure is correct, the inverse design by optimization should be possible for the given design space. That is, once the L/D history is prescribed at a given flow condition, it should be shown that the present design procedure can find the airfoil that has the same L/D history as prescribed.

The inverse design is performed within the ranges shown in Table 3. The flow conditions are specified as

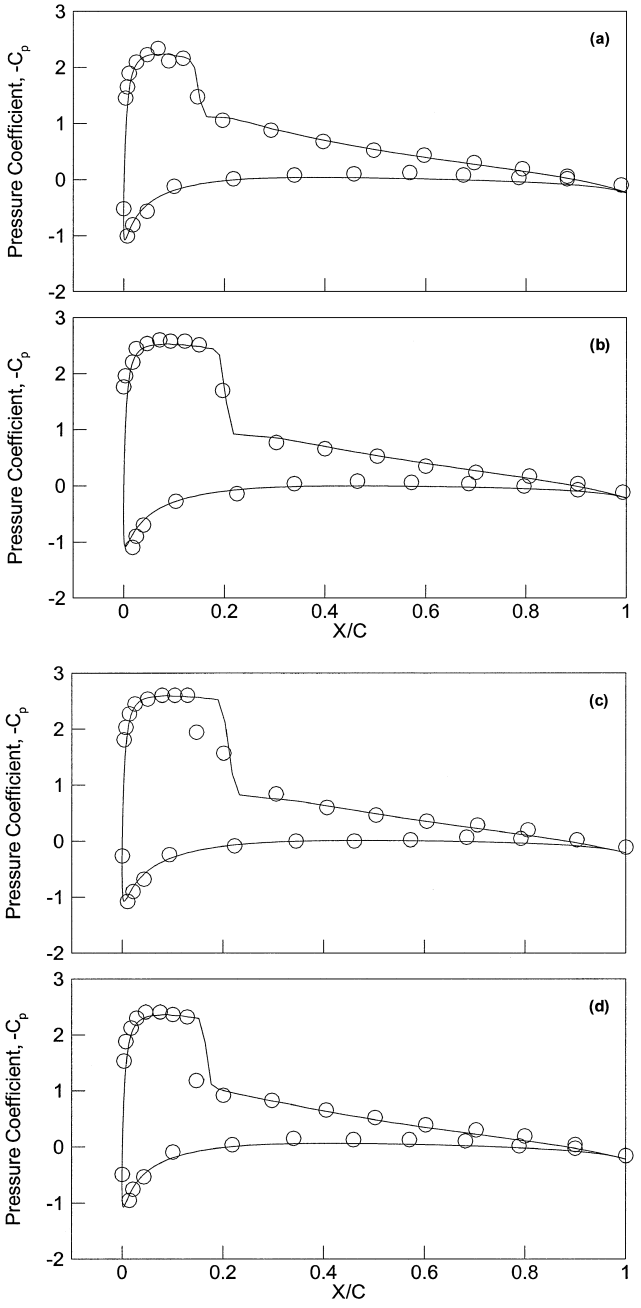

Fig. 7 Comparison of the measured and computed unsteady surface pressure coefficients for oscillatory pitching motion same parameters as Fig. 6: a) $\alpha = 5.95$ deg, up; b) $\alpha = 6.97$ deg, up; c) $\alpha = 6.57$ deg, down; and d) $\alpha = 5.11$ deg, down; ○, measured and ——, computed.

$$M_\infty = M_0 - M_m \sin(\omega t), \qquad M_0 = 0.44, \qquad M_m = 0.17$$

$$\alpha = \alpha_0 + \alpha_m \sin(\omega t), \qquad \alpha_0 = 5.5, \qquad \alpha_m = 4$$

$$k = \omega c/2U_\infty = 0.151, \qquad Re_c = 6.2 \times 10^6 \tag{14}$$

Figure 8 shows the surface pressure distributions for various phase angles during the downstroke for the given inverse design flow conditions. The baseline airfoil was used for this calculation. It is clearly shown that there is also no evidence of the dynamic stall because the amplitude of the angle of attack variation and the maximum incidence are not sufficiently high enough to incur dynamic stall.

The inverse design procedure is described as follows:

1) Unlike the inverse design for the transonic airfoil, the target L/D history is prescribed. The target history is chosen among the candidate airfoils.

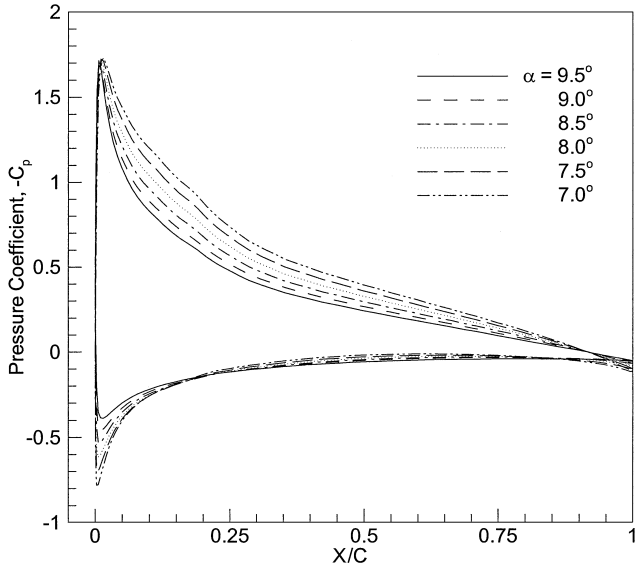

Fig. 8 Surface pressure distributions during the downstroke for the inverse design flow conditions, $M_\infty = 0.44–0.17\sin(\omega t)$, $\alpha = 5.5 + 4\sin(\omega t)$, $k = \omega c/2U_\infty = 0.151$, and $Re_c = 6.2 \times 10^6$.

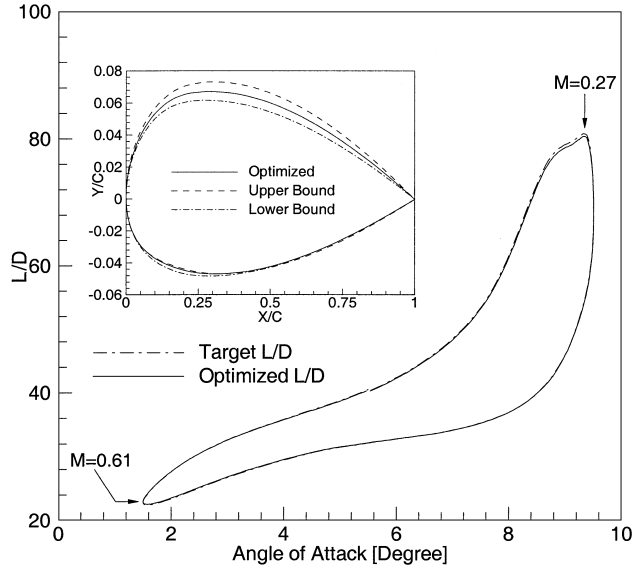

Fig. 9 Comparison between the target L/D and L/D of the inverse designed airfoil, same parameters as Fig. 8.

2) The objective function for inverse design is defined as

$$\text{minimize}: \phi = \sum_{i=i_{\min}}^{i_{\max}} \left[\left(\frac{L}{D} \right)^*_i - 1 \right]^2 \tag{15}$$

where the superscript asterisk indicates that the value is normalized by the target L/D and $i_{\min}$ ($i_{\max}$) is the starting (end) point of a cycle.

3) The RS model for the objective function is constructed after 50 numerical calculations are made for the different airfoils. The adjusted R^2 of the RS model is 0.99724, which guarantees the sufficient accuracy of the model.

4) The objective function is minimized by genetic algorithm.

Figure 9 shows the target and optimized L/D history. The L/D history of the optimized airfoil agrees very well with the target history except near the maximum phase angle. The result implies that the accuracy of the RS model and the present design procedure are reliable enough for direct numerical optimization.

Comparison Between Static Three-Point Design and Present Design Approach

This section describes the comparison between the static three-point design and the present design approach. To this end, the objective functions and constraints are defined first, and then the advantages of the present approach are shown.

In transonic airfoil design, the L/D or drag is commonly used as an objective function. However, the definition of the objective function may take different formulations with various design purposes. For a static three-point design, the summation of L/Ds obtained through the steady analysis at three different azimuth angles is usually chosen for the objective function, as in Ref. 7. If the L/D of the rotor airfoil is increased, the required power for the hovering and forward flight is reduced, and with this remaining power, the forward flight velocity could be increased. The maneuverability also could be improved, and thereby, the total performance of the helicopter could be improved. The constraints are imposed on the lift and moment coefficients to meet the goal that the performance of a designed airfoil should be at least as good as that of a baseline airfoil. Formally, the objective function and constraints for the static three-point design are given as follows: Maximize

$$F_o = \sum_{i=1}^{3} \left(\frac{L}{D} \right)^*_i \tag{16}$$

subject to

$$C^*_{l^i} > 1, \qquad \left| C^*_{m^i} \right| < 1, \qquad (i = 1, 2, 3) \tag{17}$$

where subscripts $i = 1, 2, 3$ are azimuthal locations at $\psi = 90$, 180, and 270 deg, respectively, and the superscript asterisk means that the aerodynamic values are normalized by the baseline values.

As mentioned earlier, in the static three-point design, the aerodynamic performance of the airfoil is evaluated only at several discrete azimuthal locations. Hence, it is not possible to account for properly the unsteady effects induced by the motion of an airfoil and local variations in velocity. Therefore, the objective function and constraints must be defined in a different way so that they may include the unsteady aerodynamic effects due to unsteady airfoil motion and flow conditions. In the unsteady design approach, a new objective function and constraints are devised and defined as follows. Maximize

$$F_o 1 = \frac{\int_{t_1}^{t_2} w1 \cdot (L/D)^* \, \mathrm{d}t}{\int_{t_1}^{t_2} w1 \, \mathrm{d}t}, \qquad w1 = 0.0875 \times (1.5 - \alpha) + 1 \tag{18}$$

subject to

$$F_c 1 = \frac{\int_{t_1}^{t_2} C^*_l \, \mathrm{d}t}{t_2 - t_1} > 1, \qquad F_c 2 = \left| \frac{\int_{t_1}^{t_2} C_m \, \mathrm{d}t}{\int_{t_1}^{t_2} (C_m \text{ of baseline}) \, \mathrm{d}t} \right| < 1 \tag{19}$$

where t_1 (t_2) is the time at which one period of motion starts (ends). At first, the linear weighting function, $w1$ was not included in the objective function. However, the local performance of the unsteady design at the advancing side ($\alpha = 1.5$ deg) was found to be poor even though overall dynamic performance was better than that of the three-point design result. The reason for this poor performance is that the performance of the unsteady design approach increased on the retreating side. That is, in the unsteady design, the variation of L/D due to the geometric perturbation of an airfoil is dominant near the retreating side, and the performance increase is thereby concentrated on the retreating side. To correct this imbalance, a linear weighting function was introduced so that the dynamic performance was evaluated with equal weighting at every azimuthal location. The linear weighting function $w1$ has been tuned by trial and error and specified to have 1 on the advancing side and 0.3 on the retreating side.

The objective function of the unsteady design is defined as the time average of the L/D multiplied by the weighting function over a single cycle. The lift constraint means that the time average of the normalized lift must be greater than that of the baseline airfoil.

The pitching moment constraint means that the absolute value of the time-averaged pitching moment should be less than that of the baseline airfoil. This keeps the designed airfoil from having excessive positive or negative pitching moment.

There are 50 numerical experimental points that satisfy the D-optimality condition selected using the DOPT code. Numerical experiments are then performed to construct the RS models for the objective functions and constraints. After constructing the full RS models, regression analyses are executed to identify the dominant terms, as well as to remove the unnecessary terms from the full RS models. The adjusted R^2 and standard error are summarized in Table 4. Because the adjusted R^2 of the reduced model is slightly different from that of the full model, only the full models are shown for brevity. The adjusted R^2, a measure of the model accuracy, shows satisfactory results for all RS models. The adjusted R^2 of $(L/D)_1^*$ is relatively smaller than that of the other models. The reason for this is that the Mach number on the advancing side, 0.731, belongs to the transonic flow regime, where the nonlinear effects are dominant. This nonlinearity has a tendency to decrease the prediction accuracy of the RS model.

The full RS models are exclusively used for numerical optimization because the difference of the adjusted R^2 between full and reduced models is negligible. One of the advantages of RSM is that it enables a designer to identify the dominant design variables by investigating the regression analysis results shown in Table 5. Once the dominant variables are known, they can be used as a useful guide for the future design. All linear terms are found to be important, but the camber position and leading-edge radius are less important in the quadratic terms. Based on the number of the design variables in the reduced RS models, the maximum thickness and camber are thought of as dominant variables as expected.

The resulting airfoils of the three-point design and the unsteady design are compared in Fig. 10 and the corresponding geometric parameters are summarized in Table 6. As shown in Fig. 10, the geometric perturbation from the baseline is relatively small. The maximum cambers of the three-point design and unsteady design are 1.22 and 1.33%, respectively, which lie in the reasonable ranges compared with the other currently used airfoils.[2]

Table 4 Results of regression analysis for full RS models

RS model	R^2	Adjusted R^2	Standard error
$(L/D)_1^*$	0.95503	0.92506	0.04757
$(L/D)_2^*$	0.99838	0.99709	0.00292
$(L/D)_3^*$	0.99745	0.99576	0.00596
$C_{l^1}^*$	0.99956	0.99927	0.00886
$C_{l^2}^*$	0.99998	0.99996	0.00086
$C_{l^3}^*$	0.99988	0.99980	0.00119
$C_{m^1}^*$	0.99967	0.99945	0.02916
$C_{m^2}^*$	0.99983	0.99971	0.01654
$C_{m^3}^*$	0.99995	0.99991	0.01025
F_o1	0.98265	0.96876	0.01637
F_c1	0.99803	0.99653	0.00823
F_c2	0.99439	0.98989	0.16644

Steady calculations are performed at three different flow conditions as they were done in the three-point design, and unsteady calculations are also performed to compare the static and dynamic performances of the designed airfoils. The calculated results are given in Table 7. Figures 11 and 12 show the L/D and pitching moment response of the designed airfoils, respectively. All of the values listed in Table 7 are calculated, not predicted by the RS models. The values in italic are the constraints that are actually used during the design process. It is shown that the constraints are well implemented except for the moment constraints of the three-point design at $\psi = 90$ deg and the unsteady design. As expected, the measure of the static performance, F_o, of the three-point design is higher than that of the unsteady design by 0.01. Note that the improvement of the overall static performance is mainly due to the increase in the L/D at $\psi = 90$ deg. This implies that the static performance is most sensitive to the existence of a shock wave at the advancing side, and it is possible that the static three-point design procedure may select such an airfoil to satisfy shock-free or weak-shock constraints, although the design has poor local performance at other azimuthal locations. At the advancing side ($\psi = 90$ deg), it is advantageous to retain the airfoil thickness and camber as small as possible to relieve the shock wave strength. On the other hand, the L/D has a tendency to increase with the airfoil thickness and camber at the other azimuthal locations. As shown in Table 6, the airfoil of the three-point design is thinner by 0.037% and less cambered by 0.114% compared with that of the unsteady design. As a result, the static performance of the three-point design airfoil is better at the advancing side, but at the other locations, it is slightly worse than that of the unsteady design airfoil. However, the overall static performance is better for the three-point design airfoil because the performance increase at $\psi = 90$ deg is high enough to compensate for the small increase at other locations.

For comparison of dynamic performances between the designed airfoils, F_o1 are also listed in Table 7. When F_o1 is calculated, w_1 is set to a constant. The dynamic performance improvements of the three-point design and the unsteady design are 0.027 and 0.039, respectively. Although the difference seems to be small, it is a significant improvement in that F_o1 is the time-averaged value over one cycle and the dynamic performance increase of the unsteady design is 45% greater than that of the three-point design.

Now, the question is the following: Why does the unsteady design airfoil have a better dynamic performance even though its static performance is worse than that of the three-point design airfoil? There might be three answers to this question. First, the static performance is not always proportional to the dynamic performance. In other

Table 6 Geometric values of designed airfoils

Design case	M	P	XX	I	T
Three-point design	1.2172	1.5442	11.5016	6.2200	3.5000
Unsteady design	1.3311	1.6649	11.5381	6.2200	3.5000
Case 1	1.2381	1.5000	11.5508	6.2200	3.5000
Case 2	1.1898	2.0234	11.5098	6.2200	3.5000

Table 5 Important terms in RS models (interaction terms not shown)

Term	$(L/D)_1^*$	$(L/D)_2^*$	$(L/D)_3^*$	C_{l1}^*	C_{l2}^*	C_{l3}^*	C_{m1}^*	C_{m2}^*	C_{m3}^*	F_o1	F_c1	F_c2
Linear terms												
XX	•		•	•	•	•	•	•	•	•	•	•
P	•	•			•	•	•	•	•		•	•
M	•	•	•	•	•	•	•	•	•	•	•	•
I		•	•		•	•	•	•	•	•	•	
T	•	•	•	•	•	•	•		•	•	•	•
Quadratic terms												
XX^2		•	•	•	•	•		•		•	•	
P^2		•						•				
M^2	•	•	•	•			•			•	•	
I^2												
T^2		•			•	•		•	•		•	

Table 7 Steady and dynamic performance comparison data

ψ, deg	L/D^*	C_l^*	C_m^*	F_o	F_c1	F_c2	F_o1 ($w_1=1$)
			Three-point design				
90	1.168946	*1.060994*	*1.060994*				
180	1.001955	*1.010297*	*0.999483*	3.174999	1.008129	0.848548	1.026576
270	1.004098	*1.001592*	*0.956165*				
			Unsteady design				
90	1.151010	1.103642	1.208538				
180	1.007053	1.027346	1.183586	3.164771	*1.026580*	*1.104921*	1.038519
270	1.006618	1.012013	1.111753				
			Case 1				
90	1.165373	*1.067407*	*0.979664*				
180	1.002759	*1.013060*	*1.001733*	3.173197	1.011593	0.845918	1.028877
270	1.005065	*1.003344*	*0.960326*				
			Case 2				
90	1.186231	1.045201	1.185106				
180	0.999921	1.008133	1.161834	3.188428	*1.005915*	*1.115295*	1.026251
270	1.002276	1.000755	1.084687				

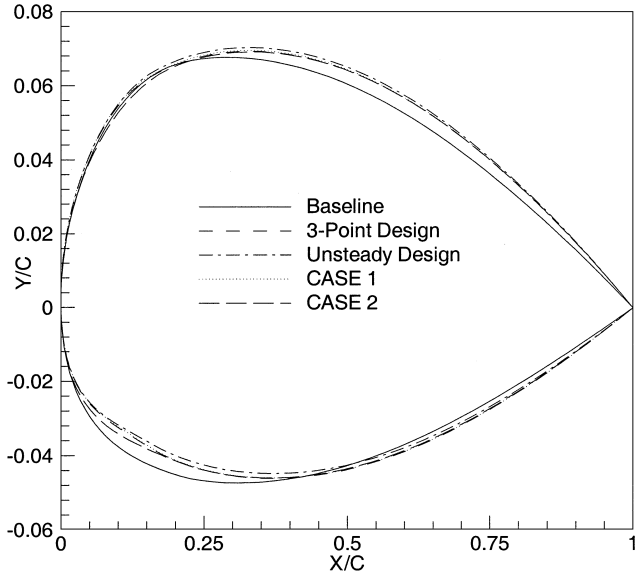

Fig. 10 Shapes of the optimized and baseline airfoils.

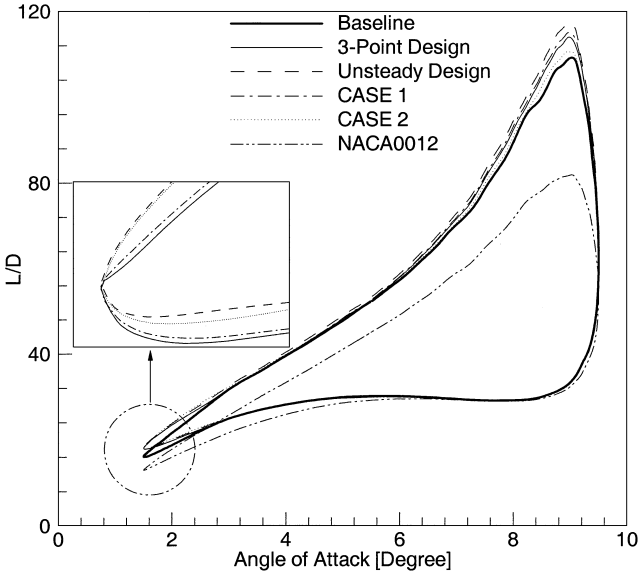

Fig. 11 Comparison of the *L*/*D* with respect to design method, same parameters as Fig. 4.

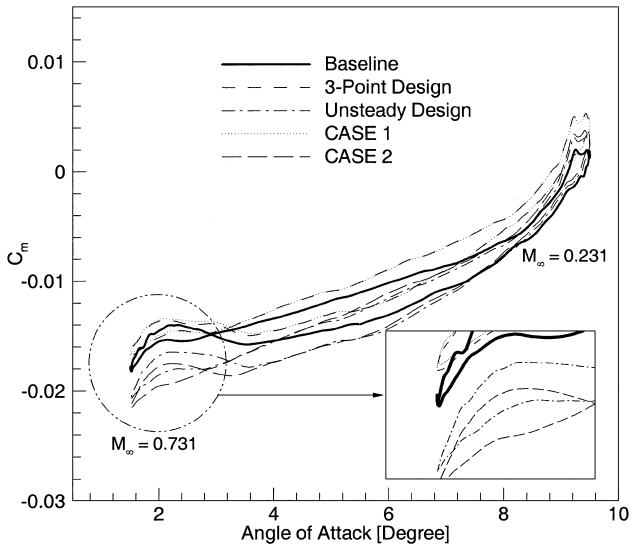

Fig. 12 Comparison of the pitching moment coefficient with respect to design method, same parameter as Fig. 4.

words, better static performance of an airfoil does not guarantee better dynamic performance. It is clearly shown in Fig. 11 that the unsteady design airfoil has higher L/D even at the advancing side ($\alpha = 1.5$ deg). Hence, one conclusion to draw is that the aerodynamic design of a body in motion should be based on the unsteady calculation results and analyses.

Second, in the three-point design, the design aerodynamic performances are evaluated at discrete points. Hence, if the performance increase at a certain point is dominant, the design result is implicitly overweighted at that point. Hence, even if the resulting airfoil of the three-point design has a better static performance than that of the unsteady design, its overall dynamic performance could be worse compared with that of the unsteady design in which the performance is continuously evaluated with even weight.

Third, the moment constraints used in the three-point design are too tight to allow enough variation of the design variables. As shown in Table 7, the F_c2 of the three-point design airfoil is only 0.849, which means that there is still enough margin to improve the dynamic performance of the airfoil in view of the unsteady moment constraints. More specifically, it is possible that even the allowable airfoils in terms of the dynamic moment constraint may be excluded during the three-point design process.

The moment constraints are violated in both the three-point design and the unsteady design. The prediction accuracy of the RS model may be reduced due to the nonlinear characteristics of the transonic flowfield. Because the RSM is a statistical approach, some

prediction error is inevitable but can be alleviated by increasing the number of numerical experiments. For the three-point design airfoil, the moment constraint is violated by 6% at $\psi = 90$ deg, and for the unsteady design airfoil, the dynamic moment constraint F_c2 is violated by 10%. Hence, it should be confirmed that the better dynamic performance of the unsteady design airfoil is not due to the greater violation of the moment constraints because the excessive pitching moment generally indicates more camber and thickness of the airfoil that has a better performance in a subsonic flowfield. Accordingly, two additional cases were calculated to clarify the independent roles and characteristics of the objective function and constraints. Case 1 represents the combination of the objective function of the unsteady design and the constraints of the three-point design, whereas, in case 2, the objective function of the three-point design is used together with the constraints of the unsteady design.

The case 1 resulting airfoil is slightly thicker and more cambered than the three-point design airfoil. The static performance is almost the same as that of the three-point design airfoil, whereas its dynamic performance is slightly higher by 0.2%. This result implies that when using the same pitching moment constraint as in the three-point design, the design result is practically independent of the definition of objective function.

In case 2, the increase in static performance is more concentrated at $\psi = 90$ deg than in the three-point design, and the overall static performance F_o is the greatest. On the other hand, the dynamic moment constraint F_c2 is violated by 11.53%. That is, the allowable limits of the dynamic moment constraint are almost the same as those of the unsteady design. However, F_o1 of case 2 is the smallest of all cases. This means that the dynamic performance is not always better in spite of the greater violation of the dynamic moment constraint. From the preceding results, it is found that the dynamic performance improvement is the greatest in the unsteady design because it allows enough spaces within which design variables can move, satisfying the constraints, and the unsteady effects are correctly included in the objective function.

The unsteady design also could improve the hovering performance of the rotor airfoil. The hovering flight conditions are essentially the steady-state flight conditions, and they are implicitly included in the unsteady design flow conditions. There is another way of including the hovering performance in the present design method. After the hovering performance is calculated using the steady numerical analysis code, the objective function can be recomposed by adding hovering performance such as L/D to the objective function of the unsteady design. After this, the recomposed objective function is maximized to find the optimal airfoil under the appropriate constraints. This approach handles a multi-objective problem, and it might give a reasonable optimization result.

Determination of Specific Design Point by Introducing New Weighting Function

Another advantage of our unsteady design approach is that, by introducing an adequate weighting function, a designer can easily determine a specific azimuthal location at which the airfoil characteristics are optimized. To achieve this goal, a new weighting function is introduced, and the objective function is modified as follows. Maximize

$$F_o2 = \frac{\int_{t_1}^{t_2} w(\alpha, \alpha_{\text{ref}}) \cdot (L/D)^* \, \mathrm{d}t}{\int_{t_1}^{t_2} w(\alpha, \alpha_{\text{ref}}) \, \mathrm{d}t}$$

$$w(\alpha, \alpha_{\text{ref}}) = w1 \cdot w2(\alpha, \alpha_{\text{ref}})$$

$$w2 = w2(\alpha, \alpha_{\text{ref}}) = \frac{0.7}{1 + |\alpha - \alpha_{\text{ref}}|^3} + 0.3 \qquad (20)$$

The weighting function $w2(\alpha, \alpha_{\text{ref}})$ has its maximum at $\alpha = \alpha_{\text{ref}}$, and the magnitude decreases exponentially elsewhere. The shapes of the weighting functions $w(\alpha, \alpha_{\text{ref}})$ with respect to α_{ref} are shown in Fig. 13. When a weighting function is defined this way, a designer can specify an azimuthal location at which the performance improvement is concentrated by changing α_{ref}. That is, if α_{ref} is

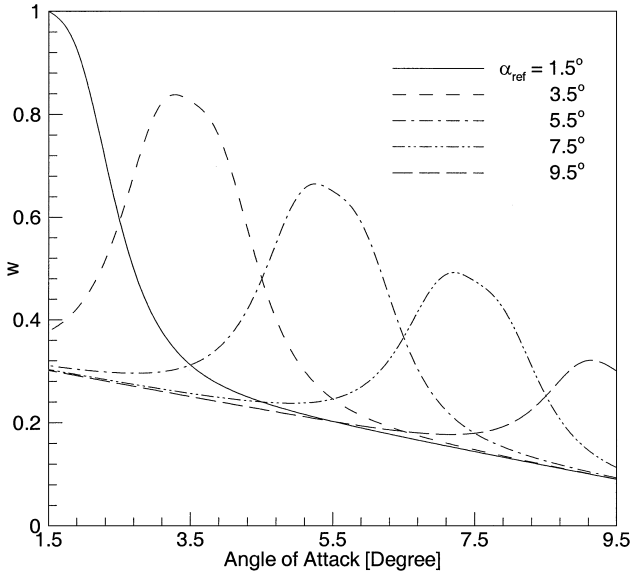

Fig. 13 Variation of the weighting function w with respect to reference angle of attack.

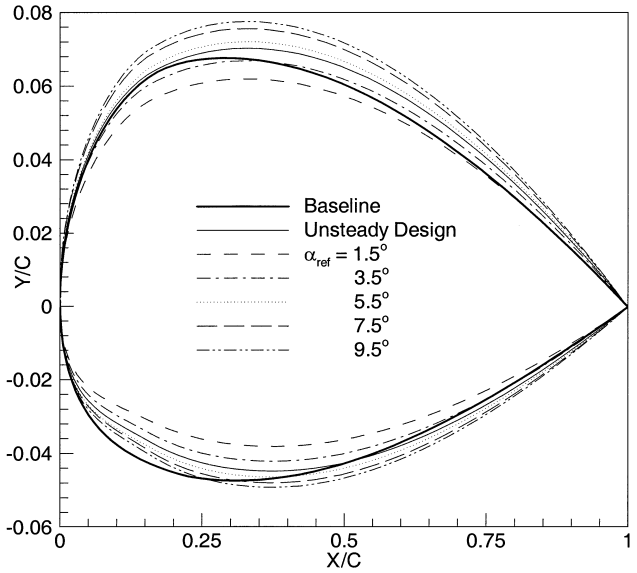

Fig. 14 Variation of optimized airfoils with respect to reference angle of attack.

1.5 deg, it means that the advancing side where the angle of attack is low and the Mach number is high is chosen as the azimuthal location at which the airfoil performance is improved intensively. In the same way, when α_{ref} is set to 9.5 deg, it means that the designer wants to optimize the airfoil characteristics on the retreating side. In this work, the modified objective function F_o2 is maximized under the same constraints as it is in the unsteady design, and optimizations are performed with respect to five different weighting functions, $\alpha_{\text{ref}} = 1.5$, 3.5, 5.5, 7.5, and 9.5 deg, to investigate the influence of the weighting.

The variations of the optimized airfoils and design variables with weighting functions are shown in Figs. 14 and 15. It is clear from Figs. 14 and 15 that the airfoils show significant variations with weightings. The variations of each design variable are also shown in Fig. 15 to clarify the effect of the weighting functions. The values of the design variables at $\alpha_{\text{ref}} = 0.0$ are obtained through the unsteady design. When $\alpha_{\text{ref}} = 1.5$ deg, which implies that the aerodynamic performance near the advancing side is the most important, the airfoil has the smallest thickness and camber. Both the thickness and camber increase as α_{ref} increases toward the retreating side. The

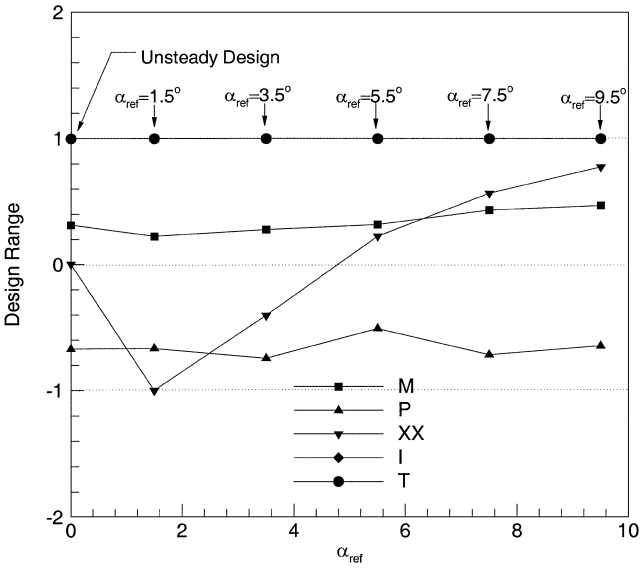

Fig. 15 Variation of the design variables with respect to reference angle of attack.

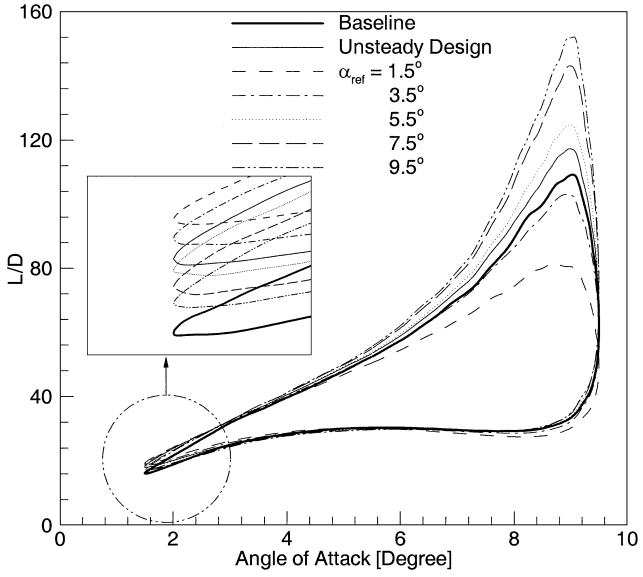

Fig. 16 Comparison of the *L*/*D* with respect to reference angle of attack, same parameters as Fig. 4.

maximum camber of all airfoils lies in the range from 1.24 to 1.48%, and it is concluded that they lie in a reasonable range compared with the other currently used airfoils.[2] The maximum thickness positions and leading-edge radii are located on the upper limits of the ranges of the design variables. This result implies that the true optima may be located outside of the specified ranges. However, the ranges of the design variables are not changed in this work because they are already in reasonable ranges, when judged from other airfoils. The results show that the quantitative behaviors of the design variables can be easily analyzed from the numerical optimization procedure.

The histories of the L/D for each optimized airfoil are shown in Fig. 16. As intended, $\alpha_{ref} = 1.5$ deg has the maximum L/D at the advancing side, whereas $\alpha_{ref} = 9.5$ deg shows the best performance at the retreating side. The results indicate that the effects of the weighting functions are correctly implemented in general.

In Fig. 17, the moment coefficient variations of the optimized airfoils are shown. The trends of the moment coefficient variation of each optimized airfoil are very similar to that of the baseline. The deviations of the moment curve of each optimized airfoil from that of the baseline airfoil show that the moment constraint is reasonably well implemented.

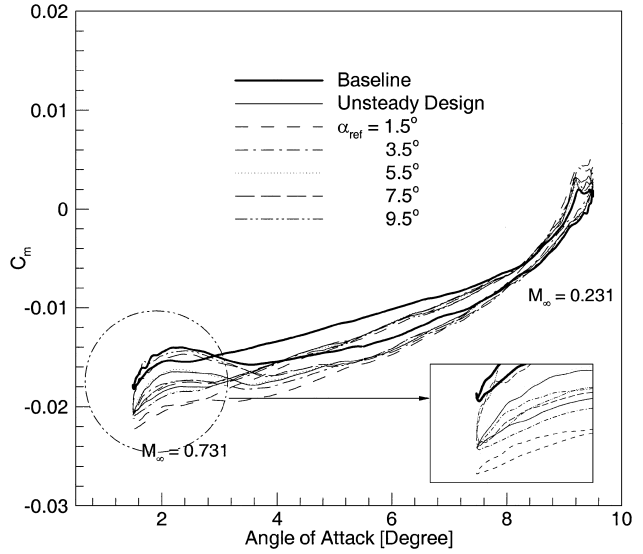

Fig. 17 Comparison of pitching moment coefficient with respect to reference angle of attack, same parameters as Fig. 4.

Conclusions

In this work, a new design procedure that can handle the dynamic response of an airfoil subjected to unsteady motion and flow conditions was suggested. For this procedure, a numerical analysis code was developed that can handle the oscillatory pitching motion of an airfoil and the inflow Mach number variation. The analyses during the design process were limited to the cases without dynamic stall because the numerical analysis code cannot predict the dynamic stall phenomena with sufficient accuracy. A new objective function was defined to represent the overall performance over a single cycle, and a weighting function was introduced to enable a designer to determine a specific azimuthal location at which the performance improvement was concentrated. To demonstrate the advantages of the present method, a static three-point design was also performed, and the design results were compared in terms of the static and dynamic aerodynamic performance. It is concluded that for the design of a body in motion, the present design procedure is more appropriate than the three-point design method: 1) Static performance is not always proportional to dynamic performance. In other words, a better static performance of an airfoil does not guarantee a better dynamic performance. Hence, the aerodynamic design of a body in motion should be based on the unsteady calculation results and analyses. 2) In the three-point design procedure, the objective function was evaluated at discrete points. Hence, if the performance increase is dominant at a certain point, the overall design result can be implicitly overweighted at that point. To avoid this problem, the objective function should be continuously evaluated with even weight, as in the present method. 3) The moment constraint suggested in the present method is more advantageous because the static moment constraint in the three-point design is too tight to allow enough variation of the design variables.

Acknowledgments

This research was supported by the Brain Korea 21 Project and Center of Innovative Design Optimization Technology [Engineering Research Center (ERC) of Korea Science and Engineering Foundation].

References

[1]Wilbey, P. G., "The Development of Rotor Airfoil Testing in the UK—The Creation of a Capability to Exploit a Design Opportunity," *Proceedings of the 22nd European Rotorcraft Forum*, The Royal Aeronautical Society, London, UK, 1996, pp. 18.1–18.11.

[2]McCroskey, W. J., McAlister, K. W., Carr, L. W., Pucci, S. L., Lambert, O., and Indergrand, R. F., "Dynamic Stall on Advanced Airfoil Sections," *Journal of American Helicopter Society*, Vol. 26, No. 3, 1981, pp. 40–50.

[3]Liiva, J., and Davenport, F. J., "Dynamic Stall of Airfoil Sections for High-Speed Rotors," *Journal of American Helicopter Society*, Vol. 14, No. 2, 1969, pp. 26–33.

[4]Gustafson, B., "The Application of Airfoil Studies to Helicopter Rotor Design," NACA TN-1812, Feb. 1949.

[5]Stivers, L. S., Jr., and Rice, F. J., Jr., "Aerodynamic Characteristics of Four NACA Airfoil Sections Designed for Helicopter Rotor Blades," NACA Rept. RB-L5K02, Jan. 1946.

[6]Kemp, L. D., "An Analytical Study for the Design of Advanced Rotor Airfoils," NASA CR-112297, March 1973.

[7]Fanjoy, D. W., and Crossley, W. A., "Aerodynamic Shape Design for Rotor Airfoils via Genetic Algorithm," *Proceedings of the American Helicopter Society 53rd Annual Forum*, AHS International, Alexandria, VA, 1997, pp. 263–270.

[8]Tapia, F., Sankar, L. N., and Schrage, D. P., "An Inverse Aerodynamic Design Method for Rotor Blades," *Journal of American Helicopter Society*, Vol. 42, No. 4, 1997, pp. 321–326.

[9]Hassan, A. A., and Charles, B. D., "Airfoil Design for Helicopter Rotor Blades: A Three-Dimensional Approach," *Journal of Aircraft*, Vol. 34, No. 2, 1997, pp. 197–205.

[10]Narramore, J. C., Nalone, J. B., and Vermeland, R., "Application of a New Navier–Stokes Inverse Method to the Design of Advanced Airfoils," *Proceedings of the American Helicopter Society 46th Annual Forum*, AHS International, Alexandria, VA, 1990, pp. 1089–1098.

[11]Yu, Y. H., Lee, S., McAlister, K. W., Tung, C., and Wang, C. U., "Dynamic Stall Control for Advanced Rotorcraft Application," *AIAA Journal*, Vol. 33, No. 2, 1995, pp. 289–295.

[12]Burgee, S., Guinta, A. A., Balalbanov, V., Grossman, B., Mason, W. H., Narducci, R., Haftka, R. T., and Watson, L. T., "A Coarse-Grained Parallel Variable-Complexity Multidisciplinary Optimization Paradigm," *International Journal of Supercomputer Applications and High Performance Computing*, Vol. 10, No. 4, 1996, pp. 269–299.

[13]Favier, D., Agnes, A., Barbi, C., and Maresca, C., "Combined Translation/Pitch Motion: A New Airfoil Dynamic Stall Simulation," *Journal of Aircraft*, Vol. 25, No. 9, 1988, pp. 805–814.

[14]Favier, D., Maresca, C., and Rebont, J., "Dynamic Stall Due to Fluctuations of Velocity and Incidence," *AIAA Journal*, Vol. 20, No. 7, 1982, pp. 865–871.

[15]Baldwin, B. S., and Lomax, H., "Thin Layer Approximation and Algebraic Model for Separated Turbulent Flows," AIAA Paper 78-0257, Jan. 1978.

[16]Sobieszczanski-Sobieski, J., and Haftka, R. T., "Multidisciplinary Aerospace Design Optimization: Survey of Recent Developtment," AIAA Paper 96-0711, Jan. 1996.

[17]Venter, G., Haftka, R. T., and Starnes, J. H., Jr., "Construction of Response Surfaces for Design Optimization Applications," *Proceedings of the 6th AIAA/NASA/ISSMO Symposium on Multidisciplinary Analysis and Optimization*, AIAA, Reston, VA, Sept. 1996, pp. 548–564.

[18]Guinta, A. A., "Aircraft Multidisciplinary Design Optimization Using Design of Experimental Theory and Response Surface Modeling Methods," Ph.D. Dissertation, Dept. of Aerospace Engineering, Virginia Polytechnic Inst. and State Univ., Blacksburg, VA, May 1997.

[19]Yee, K., Lee, D. H., and Lee, S., "Unsteady Flowfield and Noise Propagation Due to Transonic Airfoil–Airfoil Interaction," *AIAA Journal*, Vol. 36, No. 5, 1998, pp. 791–798.

[20]Landon, R. H., "NACA 0012 Oscillatory and Transient Pitching," AGARD R-702, Jan. 1982.